Hindawi
Shock and Vibration
Volume 2018, Article ID 8386428, 11 pages
https://doi.org/10.1155/2018/8386428

Research Article

Scale Effect on the Anisotropy of Acoustic Emission in Coal

Honghua Song[1,2] **Yixin Zhao**[1,2,3] **Yaodong Jiang**[3,4] **and Jiehao Wang**[2]

[1]*College of Resources and Safety Engineering, China University of Mining and Technology, Beijing, China*
[2]*Energy and Mineral Engineering, G3 Center and EMS Energy Institute, Pennsylvania State University, University Park, PA, USA*
[3]*State Key Laboratory of Coal Resources and Safe Mining, China University of Mining and Technology, Beijing 100083, China*
[4]*School of Mechanics and Civil Engineering, China University of Mining and Technology, Beijing 100083, China*

Correspondence should be addressed to Honghua Song; honghuasong8@hotmail.com

Received 2 September 2018; Revised 27 October 2018; Accepted 11 November 2018; Published 18 December 2018

Academic Editor: Roberto Palma

Acoustic emission (AE) in coal is anisotropic. In this paper, we investigate the microstructure-related scale effect on the anisotropic AE feature in coal at unconfined loading process. A series of coal specimens were processed with diameters of 25 mm, 38 mm, 50 mm, and 75 mm (height to diameter ratio of 2) and anisotropic angles of 0°, 15°, 30°, 45°, 60°, and 90°. The cumulative AE counts and energy dissipation increase with the specimen size, while the energy dissipation per AE count behaves in the opposite way. This may result from the increasing amount of both preexisting discontinuities and cracks (volume/number) needed for specimen failure and the lower energy dissipation AE counts generated by them. The effect of microstructures on the anisotropies of AE weakens with the increasing specimen size. The TRFD and its anisotropy reduce as the specimen size increases, and the reduction of fractal dimension is most pronounced at the anisotropic angle of 45°. The correlation between TRFD and cumulative AE energy in the specimens with different sizes are separately consistent with the negative exponential equation proposed by Xie and Pariseau. With the specimen size gain, the reduction of the TRFD weakens with the increasing amount of cumulative absolute AE energy.

1. Introduction

Acoustic emission (AE) is a broadly existing phenomenon regarding brittle fracture [1–4]. The AE in coal and rock has been studied for both laboratory and field uses [5–14] due to the wealth information contained in the AE signals. As natural features, both anisotropy and scale effect are also found to be present in AE in coal/rock as the loading direction and the specimen scale change [15–18]. In general, investigating the scale effect on the mechanical properties of coal and rock is beneficial for the upscaling of the laboratory experimental results to the field use [19–21]. Studying the anisotropic AE features in coal/rock is helpful in preventing the various dynamic disasters (coal bump, rock burst, and coal and gas outbursts) and mining failures. However, the interaction influence of these two factors on the AE is not investigated nor constraint in coal. Thus, in this study, the scale effect on the anisotropic AE features of coal is explored.

Scale effect and AE anisotropy are the microstructure-related phenomenon associated with mechanical responses in coal [18, 19, 21, 22]. The scale effect on the mechanical properties of coal results from the increasing amount of microstructures in a larger specimen [19, 21], while the anisotropic AE features are affected by the directional spatial distribution of these microstructures relative to the loading directions since AE signals are generated by the rapid growth and interaction of microcracks in brittle materials [17]. Therefore, obtaining the microstructural variation of specimens with different sizes is significant for the understanding of the scale effect on the AE anisotropy.

X-ray computed tomography (X-ray CT) is a non-destructive imaging and analyzing technique [23–29]. It provides the feasibility in characterizing a large variety of materials in geoscience, including cleats/fractures, minerals inclusion, and pores [21, 30–33]. Thus, the volume variation of microstructures in coal with the specimen size can be quantitatively obtained by the X-ray CT in conjunction with

the reconstruction algorithm and threshold segmentation technique.

Fractal dimension provides an approach in the characterization of the overall AE features [12, 34, 35] due to its broad correlations with other AE parameters [12, 36]. Thus, the overall scale effect on the anisotropic AE characteristics is capable of being quantitatively described by a single parameter. The spatial distribution and time sequence-related fractal dimension are two primary fractal dimension forms [35, 37–39], and they are classified by the AE count distribution needed for calculation, namely, the spatial or time sequential distribution [18, 36].

To understand the scale effect on the anisotropy of AE and investigate the possibility in upscaling usages of the laboratory AE data to analyzing of microseismic in coal mining process, a series of coal specimens are processed with diameters of 25 mm, 38 mm, 50 mm, and 75 mm (height to diameter ratio of 2) and anisotropic angles of 0°, 15°, 30°, 45°, 60°, and 90° (the orientation of bedding plane relative to the loading direction). After the microstructure characterization by X-ray micro-CT, specimens are exposed to destructive unconfined compressive tests with concurrent AE measurement. The experimental data on AE are analyzed in terms of the fractal dimension, and the correlations between the fractal dimension and energy dissipation in different specimen scales are also explored.

2. Experimental Materials and Methods

Together with the basic physical coal properties testing, coal specimens are prepared with different sizes and anisotropic angles. The AE responses of these specimens are measured under the uniaxial condition, following the interior structures characterization via X-ray micro-CT imaging.

2.1. Properties of Coal. Block coal samples were excavated from the No. 45 coal seam, which has the burst tendency, in Wudong Mine (Xinjiang Province, China). Two series of cleats can be observed in the block coal. The block coal has a density of ~1.46 g/cm^3 and a moisture content of ~1.8%. Mineral matter is present in minor proportions (8.2%), including kaolinite (62.0%), lizardite (10.8%), nacrite (26.5%), and pentahydroborite (0.4%), as defined by X-ray diffraction.

2.2. Specimen Process. Four groups of standard cylindrical specimens are prepared with the length to diameter ratio of two [40] and diameters of 25 mm, 38 mm, 50 mm, and 75 mm, respectively. For each group of coal specimens, at least nineteen specimens (spare specimen are included) are prepared with the bedding planes inclination with angles of 0°, 15°, 30°, 45°, 60°, and 90° relative to the loading direction. The coal samples and the schematic diagram of the anisotropic angles for each diameter are shown in Figure 1.

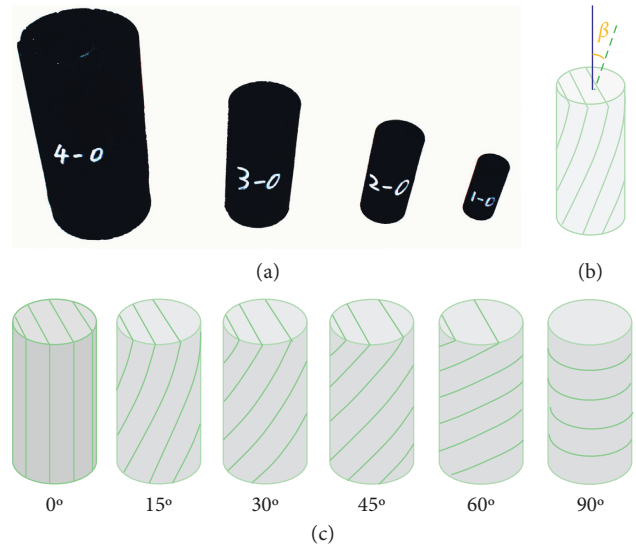

Figure 1: Specimens processed for the experiment. (a) Specimens with different diameters. (b) Schematic diagram of the anisotropic angle, β. (c) Schematic diagram of the specimens with different anisotropic angles in each specimen size.

2.3. X-Ray Micro-CT Scanning. The specimens with diameters of 25 mm, 38 mm, and 75 mm are scanned by the X-ray micro-CT to obtain the volume variation of microstructures with a change in specimen size. The X-ray micro-CT scanner used in this research is NanoVoxel 4000 (Sanying, China). It is a high-power micro-CT system using a high-voltage X-ray source (225 kV, 240 kV, and 300 kV are optional) with a submicron spatial resolution ≤0.5 μm. The voltage used here is 225 kV, and the spatial resolution is 0.5 μm.

The CT data are reconstructed by the filtered back projection Feldkamp algorithm in software VGStudio MAX 2.0 (Volume Graphics Co., Heidelberg, Germany). The median filter method is utilized for the image denoising, and the grayscale value is used as the threshold for the image segmentation in AVIZO (FEI Co., USA).

2.4. Uniaxial Compression Test and AE Measurement. Uniaxial compression tests and AE measurement are conducted after the X-ray micro-CT scanning. The uniaxial load frame has a capacity of 100 kN and a displacement precision of ±0.5%. The tests are conducted at the room temperature and controlled by displacement with a constant velocity of 0.1 mm/minute.

For the AE measurement, to obtain more AE features, four Micro30S sensors (considering the specimen size, the diameter of sensor is chosen 10 mm) and a 6-type preamplifier are used for the signal detection; the location schematic diagram of sensors is shown in Figure 2. The AE signal is recorded by a PCI-2 device (Physical Acoustic Corporation: PAC) under the waveform streaming mode. The bandwidth frequency is 1 kHz~3 MHz, having a maximum signal amplitude of 100 dB and a dynamic range greater than 85 dB. In this study, the preamplifier gain is 40 dB with a threshold of 45 dB.

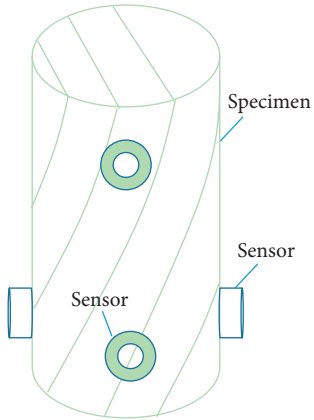

Figure 2: The location schematic diagram of the AE sensors for the AE measurement.

3. Results and Discussion

In this part, we explore the volume variation of microstructures with the increasing specimen size and investigate the microstructure-related scale effect on the AE response (counts, time, and energy) and anisotropic AE features.

3.1. CT Scanning. Mineral inclusions and preexisting discontinuities, including cracks and cleats, are two kinds of principal microstructures in coal [21, 33]. Since the grayscale of individual voxel in the X-ray CT image is a direct indication of the material density, it is thus used as a threshold to distinguish the image into multiple sections of materials.

The AE generation is a crack-related energy dissipation phenomenon. Thus, to understand the effect of specimen size on the AE feature of coal, the volume variation of the preexisting discontinuities with the specimen scale is investigated.

The digital nature of X-ray CT images facilitates the components evaluation in coal. In this study, X-ray CT images obtained from specimens 4–45 is used for the specimen reconstruction, and the grayscale value is chosen as a threshold to separate the cleats (value range 0~57) from other materials in coal, as shown in Figure 3. The voxels at this gray value range is calculated using the Avizo Volume Fraction module (Thermo Fisher Scientific and FEI, Avizo User's Guide, 2013, https://www.fei.com/software/avizo-3d-user-guide.pdf) and compared with the whole digital volume of a specimen to obtain the cleats volume.

Obviously, two series of cleats exist in the coal sample, one is parallel to the bedding plane and another one is perpendicular to the bedding plane, and they increase with the specimen size gain, as shown in Figure 3. Based on the volume evaluation methodology mentioned above, the volume variation of the preexisting discontinuities as the specimens diameter increases from 25 to 75 mm is summarized in Figure 4.

Obviously, as the specimen diameter gains from 25 mm to 75 mm, the volume of preexisting discontinuities increases from 10.07 mm^3 to 1456.08 mm^3, which is consistent with the estimation of Bieniawski [19] and variation

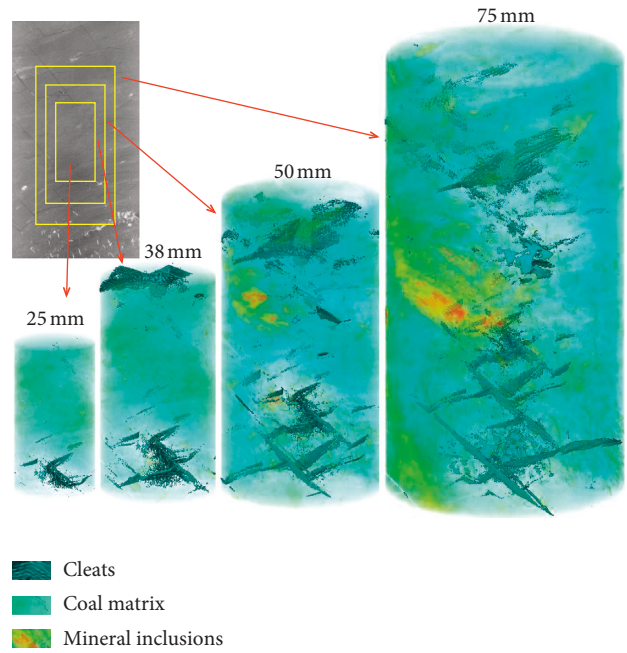

Figure 3: The volume variation of preexisting discontinuities with the specimen size.

described by Song et al. [21]. However, the volume density of preexisting discontinuities increases with the specimen diameter and the increment is minimal as the specimen diameter gains from 50 to 75 mm. This may result from the artificial selection of drilling positions during the specimen processing—positions with less discontinuities are preferred when small specimens are drilled to ensure their intactness. Meanwhile, this also a reason for that the volume increment of preexisting discontinuities is less pronounced at the diameter range of 25~38 mm than that at 38~75 mm.

3.2. Scale Effect on the AE Features. The effects of specimen size on the AE features of coal are investigated in this part, based on the measurement of four sensors. The AE count and energy dissipation used in the laboratory experiment correspond to the microseismic event and energy dissipation in microseismic activities [36]. They are primary parameters on the AE activities in both laboratory and filed work. The variation of AE counts and energy dissipation provides the precursor information of various failures during the loading process in coal and rock [41, 42], and the microseismic event and energy dissipation are still the primary parameters in the dynamic disaster preventing (coal bump and rock burst) [43–45] and the analysis of earthquake and various microseismic activities [46, 47].

The fractal features are naturally existing in the laboratory AE experiments and the field microseismic activities [12, 34, 35]. Fractal dimension calculated based on the distribution of AE counts reveal the overall features of AE counts distribution, energy release, and specimen failure. Correlations between fractal dimension and energy dissipation during the coal mining process is broadly used in the characterization and dynamic failure prediction [12, 37, 48].

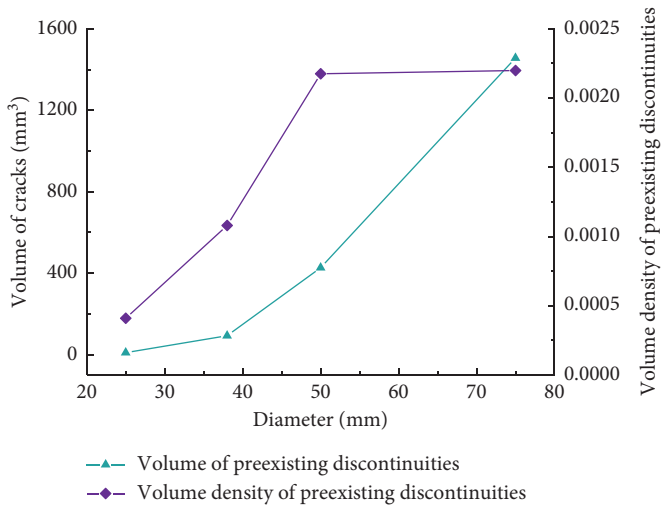

Figure 4: Variation of the volume of preexisting discontinuities with specimen diameter.

Thus, the fractal dimension also provides the feasibility in expanding the laboratory experimental results to the fieldwork, if the correlation of the fractal dimension and energy dissipation between the two scales are established.

The RA (the rise time over the amplitude), AF (the ratio of threshold crossings over the duration of the signal), frequency, amplitude, and signal duration are also the acoustic emission parameters. Analyzing these parameters allows researchers to understand the energy release (amplitude and frequency) [41, 49–51] and even the crack failure patterns (RA and AF) [52, 53] during the failure process. However, the specimen size has limited effect on the failure patterns of coal and rock [19, 54–56], and the overall failure features revealed by these parameters cannot be represented by a single value as fractal dimension and connect the laboratory experiment and the filed work. Thus, these parameters are not discussed in the research.

Considering factors above, the AE count, energy, and fractal dimension are used to expand these experimental AE results to the fieldwork. The cumulative AE counts increase from 4.80×10^5 to 1.40×10^6, as the specimen diameter gains from 25 mm to 75 mm, and the increasing forms are shown in Figure 5. Two factors may contribute to this variation with the increasing specimen size: (1) the AE generation is favored by the reducing the threshold stress for the crack initiation caused by the decreasing uniaxial compressive strength [6, 57, 58] together with the increasing amount of preexisting discontinuities and (2) the increasing amount of deformation needed for the specimen failure in a larger specimen extends the loading time and increases the AE monitoring duration, as shown in Figure 6.

The cumulative absolute AE energy also increases with the specimen size. It rises from 1.35×10^9 aJ to 2.75×10^9 aJ, as the specimen diameter gains 75 mm from 25 mm. While the average absolute AE energy per AE count decreases with the specimen size, from 2808.39 aJ/count (D = 25 mm) to 1970.28 aJ/count (D = 75 mm), the variation features of cumulative absolute AE energy and the average AE energy per count are shown in Figure 7.

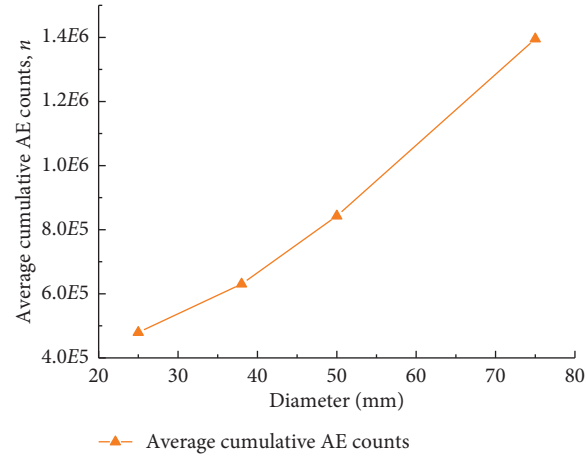

Figure 5: Variation of the average cumulative AE counts with specimen diameter.

The increasing amount of cumulative absolute AE energy can be attributed to the increment of cumulative AE counts and the greater energy dissipation caused by more deformation energy accumulation in a larger specimen since more AE counts and greater cumulative absolute AE energy are observed before the peak strength in the larger specimen, as shown in Figure 7 (here, specimens with an anisotropic angle of 90° is plotted, considering the paper length). However, reducing average absolute AE energy per AE count may be related to the increment of lower energy dissipation AE counts, which are generated by the greater amount of preexisting discontinuities and cracks needed for specimen failure in a larger specimen. However, due to the difficulties in conjunction with the AE events and energy dissipation with the crack length, orientation, and type (preexisting or newly generated), thus, we cannot give a further discussion on the physical correlation between AE counts and energy dissipation.

In addition, considering the volume changes of preexisting discontinuities per volume and the increment of cumulative AE energy and absolute AE energy, the

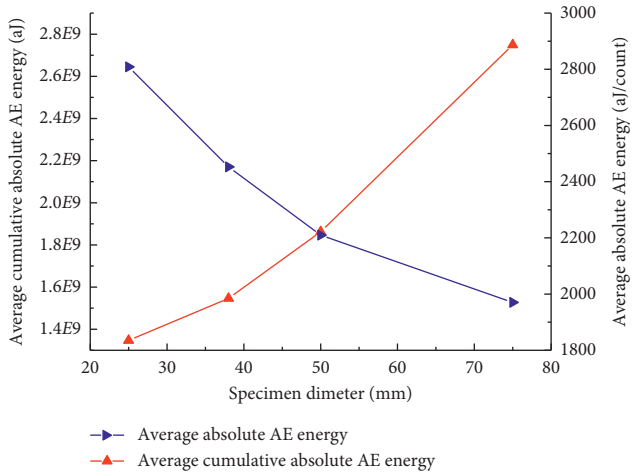

Figure 6: Variation of AE counts and cumulative absolute AE energy with the loading time and the stress during the loading process: (a) 25 mm; (b) 38 mm; (c) 50 mm; (d) 75 mm.

cumulative AE counts and absolute AE energy may have a regular increment with the specimen diameter after the specimen size greater than a certain value.

3.3. Anisotropy of AE Features Affected by Specimen Size. The scale effect on mechanical properties of coal is anisotropic [21]. In this part, the anisotropy of cumulative AE counts and absolute AE energy are explored in specimens with different sizes and anisotropic angles. The average values of these two parameters are summarized in Figures 8 and 9.

For the specimens with different anisotropic angles, the cumulative AE counts decrease to a minimum value as the anisotropic angle increases from 0 to 30°, and then it gains sharply to the maximum value at the anisotropic angle of 45° followed by a decrease until the anisotropic angle gains to 90°. In the specimen with the same size, the variation of cumulative AE counts is related to the spatial distribution of the bedding plane and face and butte cleats since they determine the time needed for specimen failure and distribution of AE counts during the loading process [21].

In general, the cumulative AE counts in specimens with different anisotropic angles gain with the specimen sizes. The increment is the most significant when the anisotropic angle is 45° (9.44×10^5), as the specimen gains from 25 mm to 75 mm, while it is minimal when the anisotropic angle is 0° (8.97×10^5). However, the variation of anisotropy of the cumulative AE counts with the increasing specimen sizes cannot be obviously observed by these curves in Figure 9.

Therefore, the variation coefficients (the ratio of the standard deviation to the mean) of cumulative AE counts in the specimens with different sizes are introduced and calculated. The result represents that the anisotropy of the cumulative AE counts reduces with the increasing specimen size since the variation coefficient reduces from 0.151 to 0.057 as the specimen diameter increases from 25 mm to 75 mm, as shown in Table 1. This indicates that the effect of the directional distribution of preexisting discontinuities on the anisotropic AE feature weakens with the increasing specimen size because of the correlation between preexisting discontinuities and AE generation. This is consistent with the anisotropy changes of uniaxial compressive strength [21].

The cumulative absolute AE energy shows a U-shape form for specimens with different anisotropic angles and is positively correlated with the uniaxial compressive strength (UCS) in the specimens with the same diameter, as we described in previous research [21]. The cumulative absolute AE energy in specimens with different anisotropic angles gains with the specimen size. The increment is more obvious as the anisotropic angle locates in the range of 30~60°, and it is maximum at the anisotropic angle of 45°.

Meanwhile, the anisotropy of cumulative absolute AE energy also reduces with the increasing specimen size, and the coefficients of variation reduce from 0.248 to 0.112 as the specimen diameter increases from 25 mm to 75 mm, as shown in Table 2. This may be due to reducing anisotropy of the UCS with the increasing specimen size because of the positive correlation between the UCS and the AE energy dissipation.

In addition, the research purpose is to focus the scale effect on the anisotropic of AE, but the specimen size has limited effect on the failure mechanisms of specimens in certain experiment [54]. Difficulties also exist in describing physical failure type (orientation/shape/length of main cracks) with a certain parameter. Thus, here we cannot give discussions and comments on relating the failure pattern with acoustic emission.

4. Fractal Features of AE in Time Sequences

Time sequence-related fractal dimension variation and the correlation of fractal dimension and energy dissipation in the specimens with different diameters are investigated.

4.1. Theoretical Development. Fractal dimension is broadly used in describing the overall AE features in brittle materials. Spatial and time sequence-related fractal dimension are the two primary forms [12, 18, 35, 37]. In this study, the anisotropic features of AE in specimens with different sizes are explored by the time sequence-related fractal dimension, based on the methodology developed by Grassberger and Procaccia (G-P) [59].

The time sequence-related fractal dimension (TRFD) is actually a correlation dimension. For a certain series of AE in time sequence with a proper time hysteresis parameter $\triangle t$, it can be extended into an m-dimensional phase space with $(N - m + 1)$ vectors that have the same time interval of $m\triangle t$. Since the AE has fractal features in time sequence, the correlation between the possibility of vector pairs (X_i, X_j) has distance of $d < l$ in the m-dimensional phase space, and l can be expressed as

$$P(l) \propto (l)^D, \tag{1}$$

where $P(l)$ is the possibility that the distance of (X_i, X_j) is less than l and D is the fractal dimension.

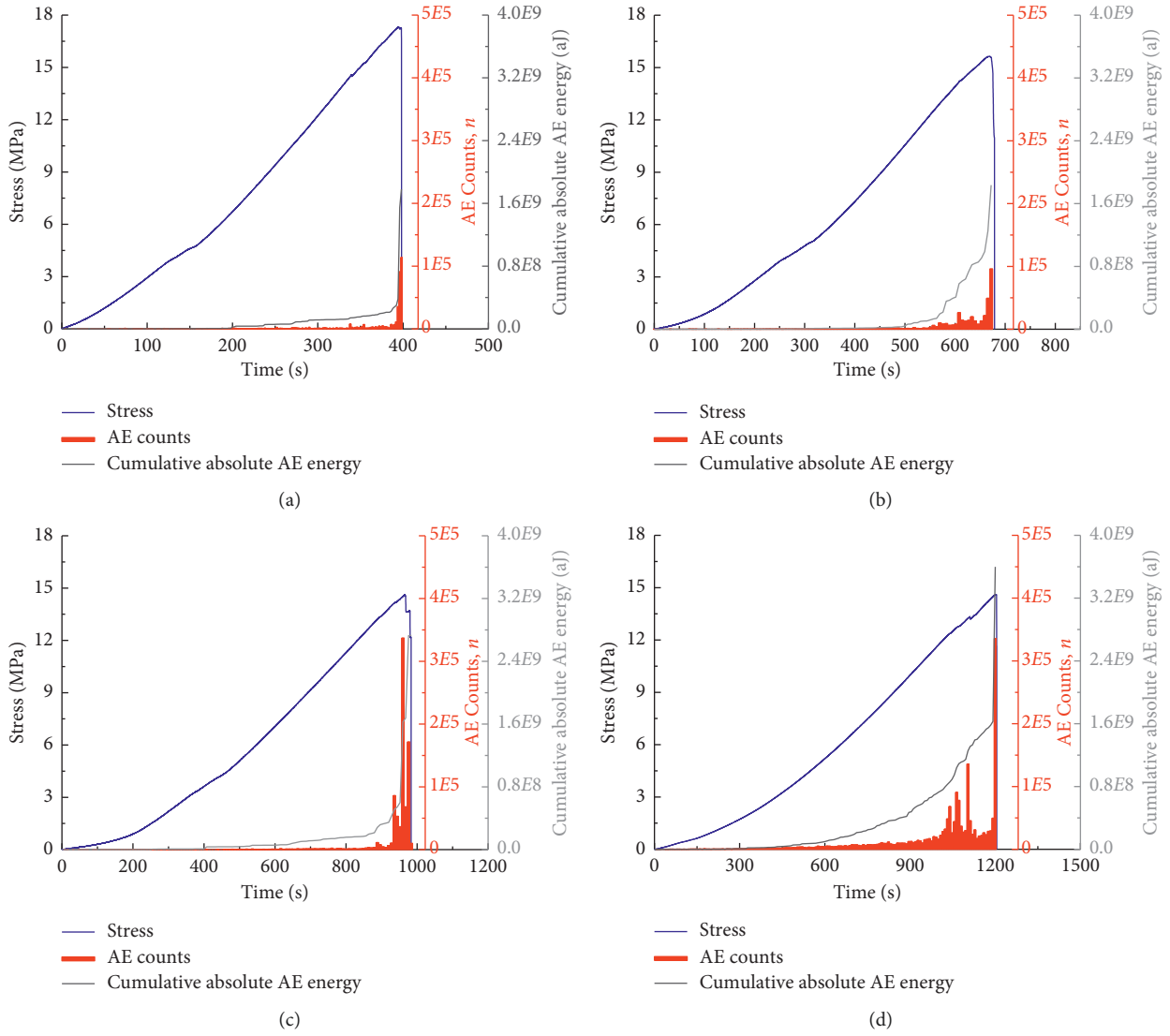

Figure 7: Variation of the cumulative absolute AE energy and the average absolute AE energy per AE count with the specimen diameter.

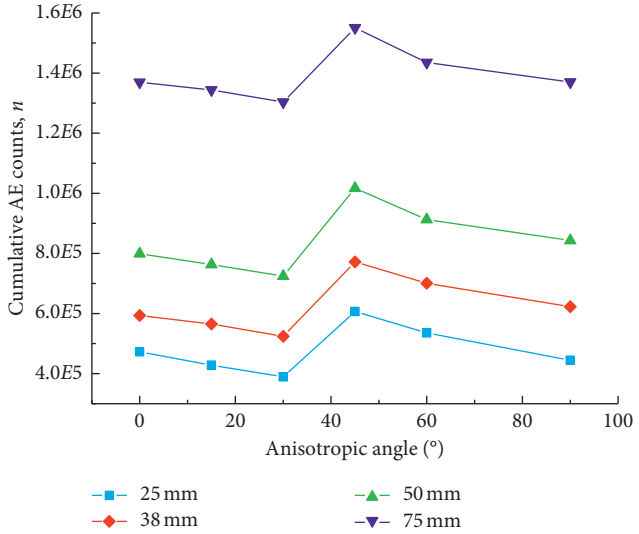

Figure 8: Anisotropy of the cumulative AE counts in the coal samples with different sizes.

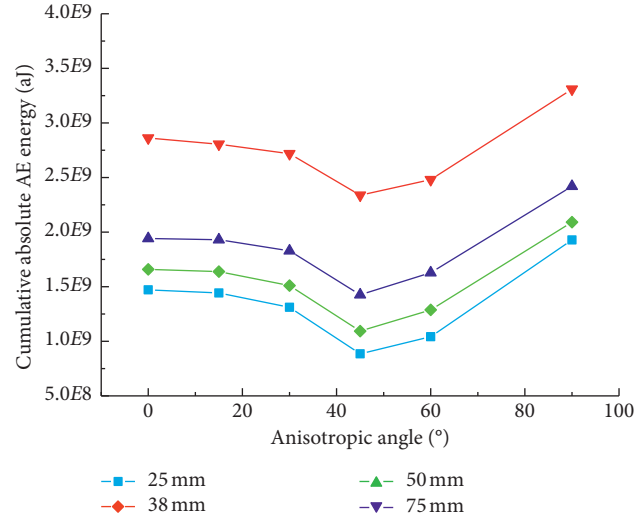

Figure 9: Anisotropy of the cumulative absolute AE energy in the specimens with different diameters.

Table 1: The variation of cumulative AE counts in the specimens with different sizes.

Specimen diameter (mm)	25	38	50	75
Average value (10^5)	4.80	6.30	8.43	13.95
Coefficient of variation	0.151	0.133	0.116	0.057

Table 2: The variation of cumulative absolute AE energy in the specimens with different sizes.

Specimen diameter (mm)	25	38	50	75
Average value (10^9aJ)	1.35	1.55	1.86	2.75
Coefficient of variation	0.151	0.133	0.116	0.057

Thus, the time sequence-related fractal dimension can be obtained by

$$D = \lim \frac{\ln P(l)}{\ln (l)}. \tag{2}$$

In general, l is obtained based on the average distance between any pair of vectors in the m-dimensional phase space, namely,

$$l = kL,$$

$$L = \frac{1}{(N-m)(N-m+1)} \sum_{i,j=1}^{i,j=N-m+1} \left\| X_i - X_j \right\| \quad (i \neq j), \tag{3}$$

where L is the average distance between any pair of vectors in the m-dimensional phase space. Accordingly, the correlation function can be expressed as

$$P(l) = \frac{1}{(N-m)(N-m+1)} \sum_{i,j=1}^{i,j=N-m+1} H\left(l - \left\| X_i - X_j \right\|\right) \quad (i \neq j), \tag{4}$$

where H is the Heaviside function ($H = 1$ when $l - \|X_i - X_j\| \geqq 0$; otherwise, $H = 0$).

In this research, m is chosen as 4, and the time interval is s. The values 0.1, 0.2, . . ., 1.2 are chosen for k, after numerous tests.

4.2. Anisotropy of Fractal Dimension in Coal. In this part, the scale effect on the anisotropic features of AE is further investigated based on the TRFD because of the overall correlations between TRFD and the AE feature during the loading process [18].

The average value of TRFD reduces with the increasing specimen size (from 1.63 to 1.41), as shown in Figure 10. This indicates that the concentration degree of AE counts before peak strength increases with the specimen size since a lower TRFD represents a greater concentration [18, 37]. In return, it verifies that the specimen size affects the distribution features of AE in time sequences.

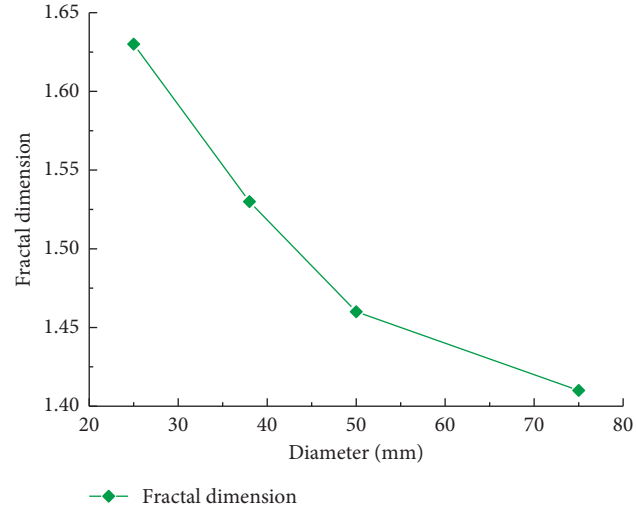

Figure 10: Variation of fractal dimension in the coal specimens with the diameter.

For the specimens with the same diameter, the TRFD has an approximate positive correlation with the cumulative AE counts, as shown in Figure 11. It reduces to a minimum value at the anisotropic angle range of 0°~15°. Then, it increases sharply to the peak at the anisotropic angle of 45°. After that, it reduces with the increasing anisotropic angle until 90°. This indicates the AE counts concentration before the peak strength during the loading process is minimal at an anisotropic angle of 45°, while it is more obvious at the anisotropic angles of 15° and 90°, based on the forgoing researches.

Meanwhile, the anisotropy of TRFD is also affected by the specimen size, and it decreases with the increasing specimen diameter. As the specimen diameter gains from 25 mm to 75 mm, the reduction of the TRFD is more obvious at the anisotropic angle range of 30°~60°, and it is most pronounced at the anisotropic angle of 45°, with a decrement of 0.44, as shown in Figure 11, while it is less obvious when the anisotropic angles are 0°, 15°, and 90°. Meanwhile, the reduction of fractal dimension decreases as the anisotropic angle is away from 45° within the anisotropic angle range of 30°~60°.

The variation of TRFD with the specimen size reveals that the scale effect on the distribution of AE counts in time sequence is greater at the anisotropic angle range of 30°~60°, while less at the anisotropic angles of 0°, 15°, and 90° because of the correlations of the TRFD and the AE distribution in time sequence. The reducing anisotropy of the cumulative AE counts also indicates the effect of directional distribution of microstructures on coal weakening with the specimen size, and this is consistent with the conclusion we obtained based on the variation of uniaxial compressive strength [21].

4.3. Correlation of Absolute AE Energy and Fractal Dimension in Specimens with Different Sizes. The correlation between the fractal dimension and the AE energy is significant for the prevention of dynamic disasters (coal bump, coal, and gas

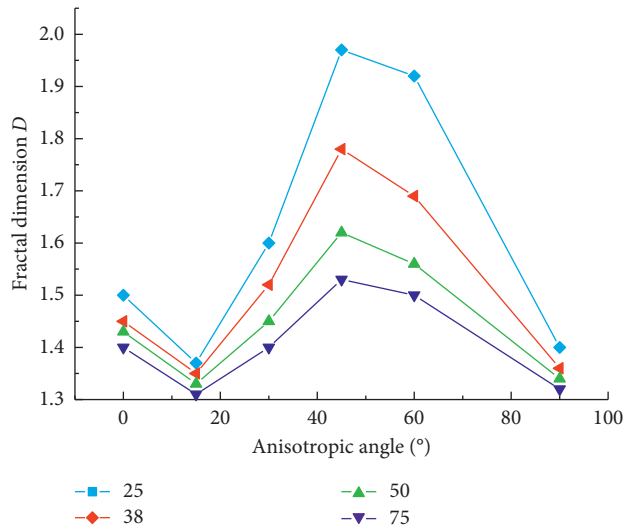

Figure 11: Fractal anisotropy in the coal specimens with different diameters.

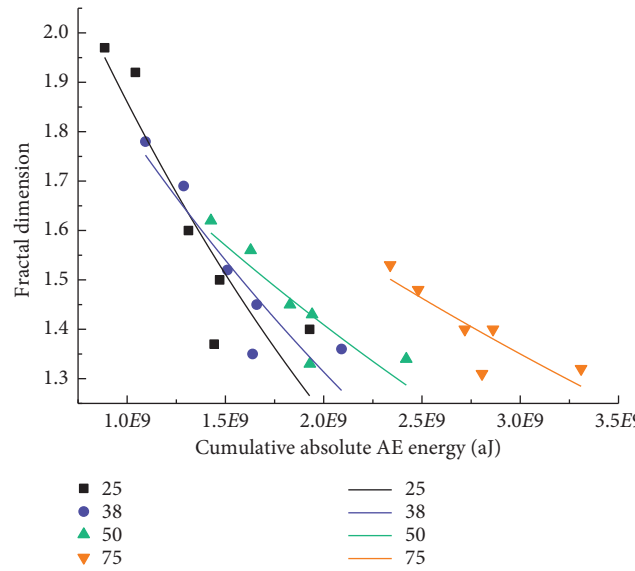

Figure 12: Correlations of fractal dimension and cumulative absolute AE energy in coal samples with different diameters.

outburst) [12, 36]. It is believed that the TRFD is negatively correlated with the cumulative absolute AE energy at the laboratory scale. Thus, the correlation of TRFD and cumulative absolute AE energy in different specimen scales is investigated to develop the approach that applies the experimental data in the field.

The empirical relation summarized by Xie and Pariseau [12] is used to analyze the correlation variation of the fractal dimension and the AE energy dissipation in specimens with different sizes:

$$D = C_1 \times \exp[-C_2 E], \quad (5)$$

where C_1 and C_2 are constants varying with region and measurement scale, the fractal dimension D ranges from 0.0 to 3.0, and E is the average AE energy released per unit area. Here, E is replaced by the average cumulative absolute AE energy, and D is the average fractal dimension in each loading direction. The regression result is shown in Figure 12; the parameters and corresponding correlation coefficients are summarized in Table 3.

The regression curves in Figure 12 agree well with the experimental data, and the correlation coefficients are greater than 0.71. This indicates the applicability of equation (1) in describing the correlation between the fractal dimension and cumulative AE energy. However, the parameters in equation (1) changes with the specimen size. The constants C_1 and C_2 in equation (1) reduce as the specimen size gains, and the reduction of fractal dimension with the cumulative AE energy decreases with the increasing specimen size.

Table 3: Constants and correlation coefficients (R^2) in specimens with different sizes.

	25 mm	38 mm	50 mm	75 mm
C_1	2.82	2.48	2.17	2.19
C_2 ($\times 10^{-10}$)	4.15	3.18	2.16	1.61
R^2	0.78	0.80	0.73	0.68

5. Conclusion

We explore the microstructure-related scale effect on the anisotropy of AE in coal, on the basis of the AE response measurement on a series of coal specimens with different diameters (25 mm, 38 mm, 50 mm, and 75 mm) and anisotropic angles (0°, 15°, 30°, 45°, 60°, and 90°). The AE response measurement is conducted under the uniaxial compressive condition, while the microstructural variations in the specimens with different sizes and anisotropic angles are characterized by the X-ray CT imaging. Meanwhile, the fractal dimensions of the AE signals of these specimens are calculated by the G-P algorithm, and scale effect on the correlations between fractal dimension and energy dissipation is also investigated. The conclusions are summarized as follows:

(a) The cumulative AE counts and absolute AE energy increase with the specimen size, while the average absolute AE energy dissipation per AE count decreases with the specimen size. This may correlate to the increasing amount of both preexisting discontinuities and cracks (volume/number) needed for specimen failure and AE counts with lower energy dissipation generated by them.

(b) The effect of directional distribution of microstructures on the anisotropic AE features weakens with the increasing specimen size. The anisotropies of AE features (cumulative AE counts and absolute AE energy) are weakened with the increasing specimen size.

(c) The value and the anisotropy of TRFD reduce with the increasing specimen size. The scale effect on the TRFD is greater within the anisotropic angle range of 30°~60° than that at the anisotropic angles of 0°, 15°,

and 90°, and it is most pronounced at the anisotropic angle range of 45°.

(d) The correlation between TRFD and cumulative AE energy in the specimens with different sizes also meet the negative exponential equation proposed by Xie and Pariseau [12], while the constants in this equation change with the specimen size. The reduction of the TRFD with the increasing cumulative AE energy reduces in the larger specimen size.

Data Availability

The data used to support the findings of this study are available from the corresponding author upon request.

Conflicts of Interest

The authors declare that they have no conflicts of interest.

Acknowledgments

This research was supported by the National Key R&D Program of China (2016YFC0801401 and 2016YFC0600708), Yue Qi Distinguished Scholar Project of China University of Mining and Technology (Beijing), and Fundamental Research Funds for the Central Universities.

References

[1] S. Barré and M. L. Benzeggagh, "On the use of acoustic emission to investigate damage mechanisms in glass-fibre-reinforced polypropylene," *Composites Science and Technology*, vol. 52, no. 3, pp. 369–376, 1994.

[2] E. Eberhardt, D. Stead, B. Stimpson, and R. S. Read, "Identifying crack initiation and propagation thresholds in brittle rock," *Canadian Geotechnical Journal*, vol. 35, no. 2, pp. 222–233, 1998.

[3] D. Lockner, "The role of acoustic emission in the study of rock fracture," *International Journal of Rock Mechanics and Mining Sciences and Geomechanics Abstracts*, vol. 30, no. 7, pp. 883–899, 1993.

[4] V. E. Tarasov, "Acoustic waves in fractal media: non-integer dimensional spaces approach," *Wave Motion*, vol. 63, pp. 18–22, 2016.

[5] D. S. Cheon, Y. B. Jung, E. S. Park, W. K. Song, and H. I. Jang, "Evaluation of damage level for rock slopes using acoustic emission technique with waveguides," *Engineering Geology*, vol. 121, no. 1-2, pp. 75–88, 2011.

[6] E. Eberhardt, D. Stead, and B. Stimpson, "Quantifying progressive pre-peak brittle fracture damage in rock during uniaxial compression," *International Journal of Rock Mechanics and Mining Sciences*, vol. 36, no. 3, pp. 361–390, 1999.

[7] D. A. Filipussi, C. A. Guzmán, H. D. Xargay, C. Hucailuk, and D. N. Torres, "Study of acoustic emission in a compression test of andesite rock," *Procedia Materials Science*, vol. 9, pp. 292–297, 2015.

[8] M. C. He, J. L. Miao, and J. L. Feng, "Rock burst process of limestone and its acoustic emission characteristics under true-triaxial unloading conditions," *International Journal of Rock Mechanics and Mining Sciences*, vol. 47, no. 2, pp. 286–298, 2010.

[9] X. Liu, M. Pan, X. Li, and J. Wang, *B-Value Characteristics of Rock Acoustic Emission Under Impact Loading*, G. Shen, Z. Wu, and J. Zhang, Eds., Springer International Publishing, Cham, Switzerland, 2017.

[10] G. Su, Y. Shi, X. Feng, J. Jiang, J. Zhang, and Q. Jiang, "True-triaxial experimental study of the evolutionary features of the acoustic emissions and sounds of rockburst processes," *Rock Mechanics and Rock Engineering*, vol. 51, pp. 375–389, 2018.

[11] V. Vishal, P. G. Ranjith, and T. N. Singh, "An experimental investigation on behaviour of coal under fluid saturation, using acoustic emission," *Journal of Natural Gas Science and Engineering*, vol. 22, pp. 428–436, 2015.

[12] H. Xie and W. G. Pariseau, "Fractal character and mechanism of rock bursts," *International Journal of Rock Mechanics and Mining Sciences and Geomechanics Abstracts*, vol. 30, no. 4, pp. 343–350, 1993.

[13] I. Yamada, K. Masuda, and H. Mizutani, "Electromagnetic and acoustic emission associated with rock fracture," *Physics of the Earth and Planetary Interiors*, vol. 57, no. 1-2, pp. 157–168, 1989.

[14] Z. Zhang, E. Wang, D. Chen, X. Li, and N. Li, "The observation of AE events under uniaxial compression and the quantitative relationship between the anisotropy index and the main failure plane," *Journal of Applied Geophysics*, vol. 134, pp. 183–190, 2016.

[15] G. Lin, Z. Wen, X. Wang, L. Chen, G. Lin, and H. Zhang, "Size effect on acoustic emission characteristics of coal-rock damage," *Advances in Materials Science and Engineering*, vol. 2017, pp. 1–8, 2017.

[16] J. Liu, M. Yang, D. Wang, and J. Zhang, "Different bedding loaded coal mechanics properties and acoustic emission," *Environmental Earth Sciences*, vol. 77, no. 8, p. 322, 2018.

[17] H. Song, Y. Zhao, Y. Jiang, and X. Zhang, "Influence of heterogeneity on the failure characteristics of coal under uniaxial compression condition," *Meitan Xuebao/Journal China Coal Soc.*, vol. 42, 2017.

[18] S. W. Zhang, K. J. Shou, X. F. Xian, J. P. Zhou, and G. J. Liu, "Fractal characteristics and acoustic emission of anisotropic shale in Brazilian tests," *Tunnelling and Underground Space Technology*, vol. 71, pp. 298–308, 2018.

[19] Z. T. Bieniawski, "The effect of specimen size on compressive strength of coal," *International Journal of Rock Mechanics and Mining Sciences & Geomechanics Abstracts*, vol. 5, no. 4, pp. 325–335, 1968.

[20] C. Gonzatti, L. Zorzi, I. M. Agostini, J. A. Fiorentini, A. P. Viero, and R. P. Philipp, "In situ strength of coal bed based on the size effect study on the uniaxial compressive strength," *International Journal of Mining Science and Technology*, vol. 24, no. 6, pp. 747–754, 2014.

[21] H. Song, Y. Jiang, D. Elsworth, Y. Zhao, J. Wang, and B. Liu, "Scale effects and strength anisotropy in coal," *International Journal of Coal Geology*, vol. 195, 2018.

[22] J. Wang, L. Xie, H. Xie et al., "Effect of layer orientation on acoustic emission characteristics of anisotropic shale in Brazilian tests," *Journal of Natural Gas Science and Engineering*, vol. 36, pp. 1120–1129, 2016.

[23] D. R. Baker, L. Mancini, M. Polacci et al., "An introduction to the application of X-ray microtomography to the three-dimensional study of igneous rocks," *Lithos*, vol. 148, pp. 262–276, 2012.

[24] V. Cnudde and M. N. Boone, "High-resolution X-ray computed tomography in geosciences: a review of the current technology and applications," *Earth-Science Reviews*, vol. 123, pp. 1–17, 2013.

[25] R. Liu and E. Sancaktar, "Identification of crack progression in filled rubber by micro X-ray CT-scan," *International Journal of Fatigue*, vol. 111, pp. 144–150, 2018.

[26] L. Mao, N. Hao, L. An, F. Chiang, and H. Liu, "3D mapping of carbon dioxide-induced strain in coal using digital volumetric speckle photography technique and X-ray computer tomography," *International Journal of Coal Geology*, vol. 147–148, pp. 115–125, 2015.

[27] J. P. Mathews, Q. P. Campbell, H. Xu, and P. Halleck, "A review of the application of X-ray computed tomography to the study of coal," *Fuel*, vol. 209, pp. 10–24, 2017.

[28] C. Puncreobutr, A. B. Phillion, J. L. Fife, and P. D. Lee, "Coupling in situ synchrotron X-ray tomographic microscopy and numerical simulation to quantify the influence of intermetallic formation on permeability in aluminium-silicon-copper alloys," *Acta Materialia*, vol. 64, pp. 316–325, 2014.

[29] N. Tsafnat, G. Tsafnat, and A. S. Jones, "Micro-finite element modelling of coke blends using X-ray microtomography," *Fuel*, vol. 87, no. 13-14, pp. 2983–2987, 2008.

[30] Y. Cai, D. Liu, J. P. Mathews et al., "Permeability evolution in fractured coal - combining triaxial confinement with X-ray computed tomography, acoustic emission and ultrasonic techniques," *International Journal of Coal Geology*, vol. 122, pp. 91–104, 2014.

[31] D. N. Espinoza, I. Shovkun, O. Makni, and N. Lenoir, "Natural and induced fractures in coal cores imaged through X-ray computed microtomography - impact on desorption time," *International Journal of Coal Geology*, vol. 154-155, pp. 165–175, 2016.

[32] C. R. Ward, "Analysis, origin and significance of mineral matter in coal: an updated review," *International Journal of Coal Geology*, vol. 165, pp. 1–27, 2016.

[33] Y. Zhao, S. Liu, G.-F. Zhao, D. Elsworth, Y. Jiang, and J. Han, "Failure mechanisms in coal: dependence on strain rate and microstructure," *Journal of Geophysical Research: Solid Earth*, vol. 119, no. 119, pp. 6924–6935, 2014.

[34] R. Zhang, F. Dai, M. Z. Gao, N. W. Xu, and C. P. Zhang, "Fractal analysis of acoustic emission during uniaxial and triaxial loading of rock," *International Journal of Rock Mechanics and Mining Sciences*, vol. 79, pp. 241–249, 2015.

[35] Z. Zhang, E. Wang, and N. Li, "Fractal characteristics of acoustic emission events based on single-link cluster method during uniaxial loading of rock," *Chaos, Solitons and Fractals*, vol. 104, pp. 298–306, 2017.

[36] H. P. Xie, J. F. Liu, Y. Ju, J. Li, and L. Z. Xie, "Fractal property of spatial distribution of acoustic emissions during the failure process of bedded rock salt," *International Journal of Rock Mechanics and Mining Sciences*, vol. 48, no. 8, pp. 1344–1351, 2011.

[37] X. Kong, E. Wang, S. Hu, R. Shen, X. Li, and T. Zhan, "Fractal characteristics and acoustic emission of coal containing methane in triaxial compression failure," *Journal of Applied Geophysics*, vol. 124, pp. 139–147, 2016.

[38] H. Takayuki, "A correlation between the b value and the fractal dimension of earthquakes," *Journal of Geophysical Research*, vol. 94, no. B6, pp. 7507–7514, 1989.

[39] R. f Yuan and Y. h Li, "Fractal analysis on the spatial distribution of acoustic emission in the failure process of rock specimens," *Int. J. Miner. Metall. Mater.*, vol. 16, pp. 19–24, 2009.

[40] ISRM, *The Complete ISRM Suggested Methods for Rock Characterization, Testing and Monitoring: 1974-2006*, International Society for Rock Mechanics, Commission on Testing Methods, Ankara, Turkey, 2007.

[41] J. Peng and S. Q. Yang, "Comparison of mechanical behavior and acoustic emission characteristics of three thermally-damaged rocks," *Energies*, vol. 11, 2018.

[42] F. Zhao, Y. Li, Z. Ye et al., "Research on Acoustic Emission and Electromagnetic Emission Characteristics of Rock Fragmentation at Different Loading Rates," *Shock and Vibration*, vol. 2018, Article ID 4680879, 8 pages, 2018.

[43] W. Cao, J. Q. Shi, G. Si, S. Durucan, and A. Korre, "Numerical modelling of microseismicity associated with longwall coal mining," *International Journal of Coal Geology*, vol. 193, pp. 30–45, 2018.

[44] Q. Wu, J. Jiang, Q. Wu, Y. Xue, P. Kong, and B. Gong, "Study on the fracture of hard and thick sandstone and the distribution characteristics of microseismic activity," *Geotechnical and Geological Engineering*, vol. 36, no. 6, pp. 3357–3373, 2018.

[45] B. Yu, J. Zhao, and H. Xiao, "Case study on overburden fracturing during longwall top coal caving using microseismic monitoring," *Rock Mechanics and Rock Engineering*, vol. 50, no. 2, pp. 507–511, 2017.

[46] B. D. E. Dando, B. S. Iranpour, L. W. Bjerrum, and V. Oye, "Real-time microseismic monitoring in the North Sea with advanced noise removal methods," *SEG Technical Program Expanded Abstracts 2016*, pp. 2657–2661, 2016.

[47] L. Smit, B. Braeuer, J. Stankiewicz, and Å. Fagereng, "Microseismic activity and basement controls on an active intraplate strike-slip fault, ceres–tulbagh, South Africa," *Bulletin of the Seismological Society of America*, vol. 105, pp. 1540–1547, 2015.

[48] D. Mondal, P. N. S. Roy, and P. K. Behera, "Use of correlation fractal dimension signatures for understanding the overlying strata dynamics in longwall coal mines," *International Journal of Rock Mechanics and Mining Sciences*, vol. 91, pp. 210–221, 2017.

[49] B. Kong, E. Wang, Z. Li, X. Wang, Y. Niu, and X. Kong, "Acoustic emission signals frequency-amplitude characteristics of sandstone after thermal treated under uniaxial compression," *Journal of Applied Geophysics*, vol. 136, pp. 190–197, 2017.

[50] Q. Lin, D. Mao, S. Wang, and S. Li, "The influences of mode II loading on fracture process in rock using acoustic emission energy," *Engineering Fracture Mechanics*, vol. 194, pp. 136–144, 2018.

[51] M. Strantza, D. Van Hemelrijck, P. Guillaume, and D. G. Aggelis, "Acoustic emission monitoring of crack propagation in additively manufactured and conventional titanium components," *Mechanics Research Communications*, vol. 84, pp. 8–13, 2017.

[52] D. G. Aggelis, "Classification of cracking mode in concrete by acoustic emission parameters," *Mechanics Research Communications*, vol. 38, no. 3, pp. 153–157, 2011.

[53] L. N. Y. Wong and Q. Xiong, "A method for multiscale interpretation of fracture processes in carrara marble specimen containing a single flaw under uniaxial compression," *Journal of Geophysical Research: Solid Earth*, vol. 123, pp. 6459–6490, 2018.

[54] H. Masoumi, S. Saydam, and P. C. Hagan, "Incorporating scale effect into a multiaxial failure criterion for intact rock," *International Journal of Rock Mechanics and Mining Sciences*, vol. 83, pp. 49–56, 2016.

[55] P.-Z. Pan, X.-T. Feng, and J. A. Hudson, "Study of failure and scale effects in rocks under uniaxial compression using 3D cellular automata," *International Journal of Rock Mechanics and Mining Sciences*, vol. 46, no. 4, pp. 674–685, 2009.

[56] C. . . Tang, L. Tham, P. K. Lee, Y. Tsui, and H. Liu, "Numerical studies of the influence of microstructure on rock failure in uniaxial compression—Part II: constraint, slenderness and size effect," *International Journal of Rock Mechanics and Mining Sciences*, vol. 37, no. 4, pp. 571–583, 2000.

[57] M. Cai, P. K. Kaiser, Y. Tasaka, T. Maejima, H. Morioka, and M. Minami, "Generalized crack initiation and crack damage stress thresholds of brittle rock masses near underground excavations," *International Journal of Rock Mechanics and Mining Sciences*, vol. 41, no. 5, pp. 833–847, 2004.

[58] L. Xue, S. Qin, Q. Sun, Y. Wang, L. M. Lee, and W. Li, "A study on crack damage stress thresholds of different rock types based on uniaxial compression tests," *Rock Mechanics and Rock Engineering*, vol. 47, no. 4, pp. 1183–1195, 2014.

[59] P. Grassberger and I. Procaccia, "Measuring the strangeness of strange attractors," *Physica D: Nonlinear Phenomena*, vol. 9, no. 1-2, pp. 189–208, 1983.